

Studies of the mechanism of the cluster formation in a thermally sampling atmospheric pressure ionization mass spectrometer

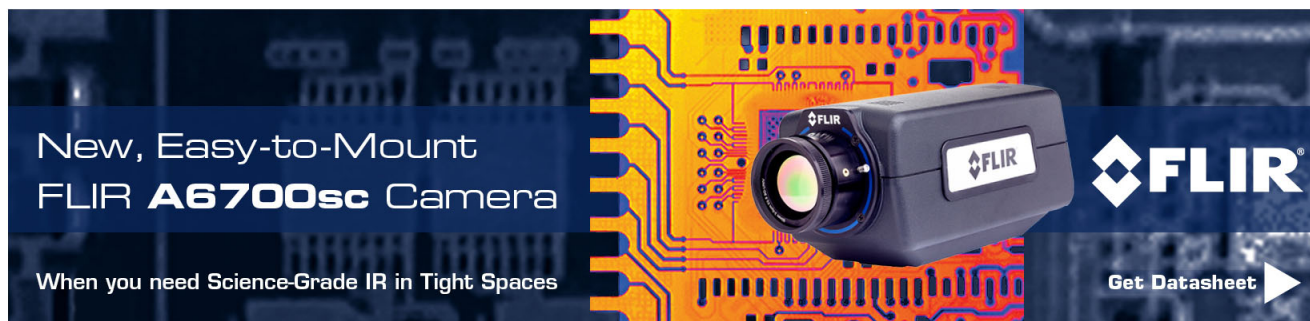
Sascha Albrecht, Sebastian Klopotoski, Valerie Derpmann, Sonja Klee, Klaus J. Brockmann, Fred Stroh, and Thorsten Benter

Citation: [Review of Scientific Instruments](#) **85**, 014102 (2014); doi: 10.1063/1.4854855

View online: <http://dx.doi.org/10.1063/1.4854855>

View Table of Contents: <http://scitation.aip.org/content/aip/journal/rsi/85/1?ver=pdfcov>

Published by the [AIP Publishing](#)



New, Easy-to-Mount
FLIR A6700sc Camera

When you need Science-Grade IR in Tight Spaces

FLIR

Get Datasheet ▶

The advertisement features a black FLIR A6700sc camera mounted on a yellow and orange printed circuit board. The background is a dark blue grid pattern. The FLIR logo is visible on the camera and in the bottom right corner.

Studies of the mechanism of the cluster formation in a thermally sampling atmospheric pressure ionization mass spectrometer

Sascha Albrecht,^{1,a)} Sebastian Klopotoski,^{2,b)} Valerie Derpmann,^{2,c)} Sonja Klee,^{2,d)} Klaus J. Brockmann,^{2,e)} Fred Stroh,^{1,f)} and Thorsten Benter^{2,g)}

¹Forschungszentrum Jülich GmbH, Institute of Energy and Climate Research, Stratosphere (IEK-7), 52428 Jülich, Germany

²Physical and Theoretical Chemistry, Institute for Pure and Applied Mass Spectrometry, University of Wuppertal, 42097 Wuppertal, Germany

(Received 2 October 2013; accepted 10 December 2013; published online 6 January 2014)

In this study a thermally sampling atmospheric pressure ionization mass spectrometer is described and characterized. The ion transfer stage offers the capability to sample cluster ions at thermal equilibrium and during this transfer fundamental processes possibly affecting the cluster distribution are also readily identified. Additionally, the transfer stage combines optional collision-induced dissociation (CID) analysis of the cluster composition with thermal equilibrium sampling of clusters. The performance of the setup is demonstrated with regard to the proton-bound water cluster system. The benefit of the studied processes is that they can help to improve future transfer stages and to understand cluster ion reactions in ion mobility tubes and high-pressure ion sources. In addition, the instrument allows for the identification of fragmentation and protonation reactions caused by CID.

© 2014 AIP Publishing LLC. [<http://dx.doi.org/10.1063/1.4854855>]

I. INTRODUCTION

Currently, atmospheric pressure ionization (API) is the method of choice for the ion generation in mass spectrometry for routine analysis. Several API methods, including atmospheric pressure photo ionization (APPI)¹ and atmospheric pressure laser ionization (APLI)² provide high analytical sensitivity and selectivity. The sensitivity and selectivity may be further improved with the proper choice of dopants since it can change the reaction cascade, which yields analyte ions or ion clusters.³ Here we present a mass spectrometer (MS) that measures ion clusters and their thermal distribution as well as other reaction products that are generated within the atmospheric pressure (AP) ion source. This powerful tool allows insights into the molecular processes of cluster formation and their fate during transmission into the mass analyzer.

Under AP conditions ion-molecule-reactions, e.g., charge transfer, addition, and substitution, cannot be avoided, thus they represent important processes that need to be understood for AP ion sources optimization. One of the most important but often neglected processes is the formation of ion bound clusters by polar species, in particular, omnipresent water molecules with both negative and positive ions.⁴ Siegel and Fite reported the detection of water ion clusters in a MS operated with very pure nitrogen, i.e., containing only a few ppmV of water.⁵ Under no circumstances should this clustering be neglected since important thermodynamic parameters such as proton affinities deviate significantly from the bare

ions to the corresponding ion bound clusters. For instance, the proton affinities of water clusters, often used as reactants in API, have been shown to increase with the number of coordinated water molecules.^{4,6} Therefore, the role of ion cluster formation in AP ion sources must be reasonably understood in order to correctly interpret the measured mass spectra and optimize the ion source performance. This is especially true with respect to quantitative analyses.

The minimal transit time of ions from an AP ion source to the collision-free region is of the order of 10 ms, results in at least 10^7 collisions of individual ions with background molecules,⁷ and therefore allots enough time for the clusters to achieve thermal equilibrium distribution. In order to avoid congested mass spectra induced by cluster formation most API MS purposefully employ electric fields in the pressure reduction stage that pushes the ion cluster equilibria toward the bare ions by collision-induced dissociation (CID).⁸ The influence of the CID on the ions should also be accounted for since it increases the ion temperature⁹ and therefore may induce further reactions in combination with the destruction of clusters. Moreover, a further increase in the ion temperature results in the fragmentation of ions.¹⁰ However, this affects the transmission efficiency of the analyzer and may lead to cross-sensitivities on the calibration factor in quantitative analysis.

In this article, we present a customized time of flight (TOF)-MS that measures the ion bound clusters, both in positive and negative ion mode. The performance of this setup is demonstrated using the proton-bound water cluster system. A study of the role of cluster formation in negative ion MS employing the ion optics and MS analyzer presented here was recently published by Derpmann *et al.*¹¹ Further cluster chemistry observed in the positive mode measurements is discussed in depth by Klee *et al.*¹²

^{a)}s.albrecht@fz-juelich.de

^{b)}s.klopotoski@uni-wuppertal.de

^{c)}v.derpmann@uni-wuppertal.de

^{d)}s.klee@uni-wuppertal.de

^{e)}brockma@uni-wuppertal.de

^{f)}f.stroh@fz-juelich.de

^{g)}tbenter@uni-wuppertal.de

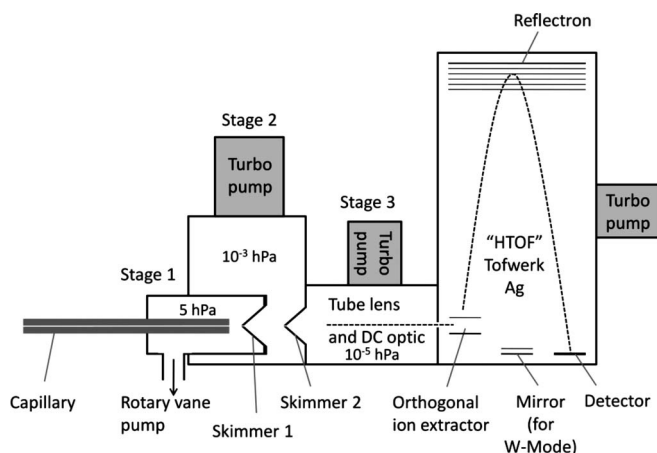


FIG. 1. A schematic drawing of the mass spectrometer.

The motivation of this work is the construction and optimization of a mass spectrometer ion sampling stage that does not significantly alter the thermal ion distribution in the API source upon transfer to the mass analyzer in order to reliably study the cluster chemistry from the ion source to the mass analyzer.

II. EXPERIMENTAL METHODS

The setup consists of an atmospheric pressure laser ionization source, a custom transfer stage, and a TOF-MS from TOFWERK AG in Thun, Switzerland. A schematic drawing of the mass spectrometer is shown in Fig. 1.

A. Ion source

The ions are produced via atmospheric pressure laser ionization in an ion source that has been described previously.^{13,14} The photon source is a diode pumped solid state (DPSS) laser operating at a wavelength of 266 nm (Cry-Las GmbH, FQSS 266-50), with a pulse duration of 1 ns, a pulse energy of 50 μ J, and a repetition rate of 100 Hz. The unfocused laser beam has a diameter of 1 mm. It is guided axially through a silica window into the ion source and then into the glass capillary ($\varnothing = 0.5$ mm, $l = 18$ cm), which is the main ionization region. Alternatively, ionization can be achieved by directing the laser beam perpendicularly into a silica capillary. In this case the signal is one to two orders of magnitude lower, but the cluster distribution remains identical. This indicates that the laser does not dissociate the generated clusters in the axial configuration.

In dopant assisted (DA) APLI toluene is often used as a dopant and reacts with the ion source matrix, generating analyte ions. The primary ions are generated in a two photon (1+1) resonance enhanced multi photon ionization (REMPI) process forming toluene radical cations.²

For all the measurements described, toluene (Sigma-Aldrich, HPLC-grade) is added at the saturation pressure to a flow of nitrogen (Linde, 99.999%). The resulting flow of gas carries toluene with a mixing ratio of 200 ppmV. Purified

water (Millipore purification system, Molsheim, France) and methanol (Sigma-Aldrich, HPLC-grade) is added in each experiment at the saturation pressure to the gas flow at mixing ratios described in Sec. IV–VI.

B. Pumping stages

The glass capillary acts as the first pressure restriction stage. The exit of the capillary in the low pressure region is wrapped with 0.25 mm diameter tantalum wire, which allows heating of the gas flow. Both ends of the capillary are metallized to provide a defined potential at the inlet and outlet. The inlet is connected to ground potential, while the outlet is either grounded or held at a defined potential.

The first pumping stage is evacuated by a 16 m³/h rotary vane pump (Oerlikon Leybold Vacuum, Cologne Germany, Tivac D16B) or by a 505 m³/h high-capacity roots blower (Oerlikon Leybold Vacuum, Cologne Germany, Ruvac Wsu 501) in combination with a 70 m³/h rotary vane pump (Pfeiffer Vacuum GmbH, Germany, Duo 65 C). A downstream pressure control system consisting of a butterfly valve (MKS Instruments Deutschland GmbH, München, Germany, MKS 253) with a built in valve controller and a capacitance manometer (MKS 626) ensures constant pressures in the range from 1 to 25 hPa in this pumping stage (cf. Fig. 1). This step is independent of the upstream gas flow.

The capillary is operated critically, with an exit plane pressure of the order of 250 hPa.⁷ The gas leaving the capillary thus forms an adiabatic expansion leading inevitably to the formation of a Mach disk. The location of the Mach disk is a function of the background pressure. In the present experiment, this location can be easily adjusted from a position upstream of the skimmer orifice to a position virtually downstream the orifice. Thus, the former “mode” represents thermal equilibrium sampling of the molecules present after the shock region. The latter “mode” leads to rapid further adiabatic cooling to very low rovibrational temperatures and resembles supersonic jet sampling (cf. Ref. 15).

The next two pumping stages are equipped with aluminum skimmers, each with an inner diameter of 0.8 mm each and a solid angle of 90° at the outer face. Skimmer 1 (cf. Fig. 1) is mounted on an insulating disk and can be electrically biased while skimmer 2 is tied to the ground potential. The differential pumping stage is equipped with a 1250 L/s turbo pump (4500 m³/h, Pfeiffer Vacuum, Asslar, Germany, TPU 1201 PC), achieving a pressure reduction of 10^{-3} hPa in the second pumping stage. The ion transfer stage downstream of the second skimmer is equipped with a 250 L/s turbo pump (900 m³/h, Pfeiffer Vacuum, Asslar, Germany, TMH 261 YP), establishing a sustained background pressure $<10^{-5}$ hPa. This stage features an ion transfer lens system which is described in detail in Sec. II D. Behind the transfer stage the ions enter the TOF analyzer through an orifice with a diameter of approximately 3 mm. The TOF is evacuated with a 250 L/s turbo pump (900 m³/h, Pfeiffer Vacuum, Asslar, Germany, TMH 261 YP) that operates at pressures $<10^{-6}$ hPa.

For measurements where the CID was kept at a minimum, the capillary outlet and both skimmers were connected to ground potential.

C. Experimental conditions in the first pumping stage

The number of ions generated in the ion source is decreased when passing through the pressure reduction stages. This reduction is proportional to the pressure drop at the nozzles if no countermeasures are taken. However, ion concentration is gained if the ions are focused into the nozzle by an electrostatic field.

Within the capillary flow the pressure drops, therefore exit port pressure is the base pressure of the following expansion. The equations required for exit pressure calculations can be found in the literature.^{16,17} Calculations show that an 18 cm long capillary with an inner diameter of 0.5 mm produces a pressure of 212 hPa at the exit port, with the upstream port held at 1013 hPa. In our experiments the pressure at the inlet was slightly higher, about 1100 hPa. Because the critical pressure depends on the pressure at the inlet, the pressure at the capillary exit increases slightly to 255 hPa.

D. Transfer lens

To guide the ions from skimmer 2 to the direct current (DC) voltage ion optical stage at the entrance of the TOF a single lens was designed employing the simulation software Simion.¹⁸ A schematic of the lens is shown in Fig. 2. Additionally, the simulated ion trajectories are included in Fig. 2 with labeled parameters of the simulation. Collisions do not play a significant role in this pumping stage (cf. Sec. VI) and thus are neglected in the simulation. The optimal voltages in the simulation fit well with the optimal voltage in the experiments ($\Delta 2$ V). The single lens consists of three tube electrodes, which have an inner diameter of 12 mm and are mounted to one fixture. Each tube electrode is connected to a voltage source by a pin attached to the outer ring of the electrode. For ease of installation, a movable tube lens extension is mounted on the first electrode to enhance collection efficiency.

Additionally, the lens system is surrounded by four electrodes. They allow the ion beam to be adjusted in x- and

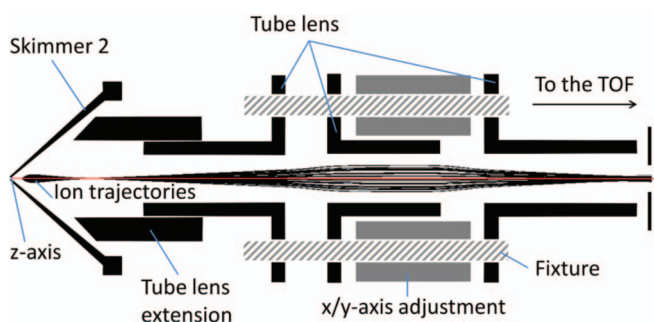


FIG. 2. A cut through of the Simion model with ion trajectories in the transfer lens system. The trajectories correspond to the following values: Skimmer 2 and x/y-axis adjustment 0 V; tube lens -70 , -20 , -70 V; positive ions (m/z 100) starting with a solid angle of 45° and 0.1 eV.

y-directions. The Simion simulations showed that, with this method, a skewed installation of less than one degree of the lens system can be corrected without any intensity loss. If the tube lens is properly adjusted these four electrodes can be grounded.

E. Time of flight mass spectrometer

A “HTOF” time of flight mass spectrometer from TOFW-ERK AG in Switzerland was employed for this study. In the current configuration it detects masses in the m/z -range >14 up to 750 with low mass discrimination since no filters (e.g., quadrupoles) are used. Using an EI (electron ionization) source even m/z 14 was detected with high intensity. All measurements presented here were obtained employing the V mode, as drafted in Fig. 1 with a mass resolution of 2500.¹⁹

III. PARAMETERS OF THE CLUSTER DISTRIBUTION

A. Theory of expansion

Figure 3 shows a schematic of the first expansion after the capillary. The gas at the end of the capillary travels at the local speed of sound (Mach number, $M = 1$) at a pressure of about 255 hPa. Thus, an under-expanded free jet forms at the exit of the capillary. Here, the internal energy and random translational energy of the molecules are converted into directed translational motion accompanied by cooling of the molecules and a decrease in the speed of sound, a , as follows from Eq. (1):

$$a = \sqrt{(\gamma RT)/m}. \quad (1)$$

R denotes the universal gas constant, T the temperature of the expanded gas, m the molar mass, and γ ($\gamma = C_p/C_v$) the heat capacity ratio.¹⁵

Since ions are efficient at driving cluster chemistry rather large clusters can be produced in the expansion. The rate of

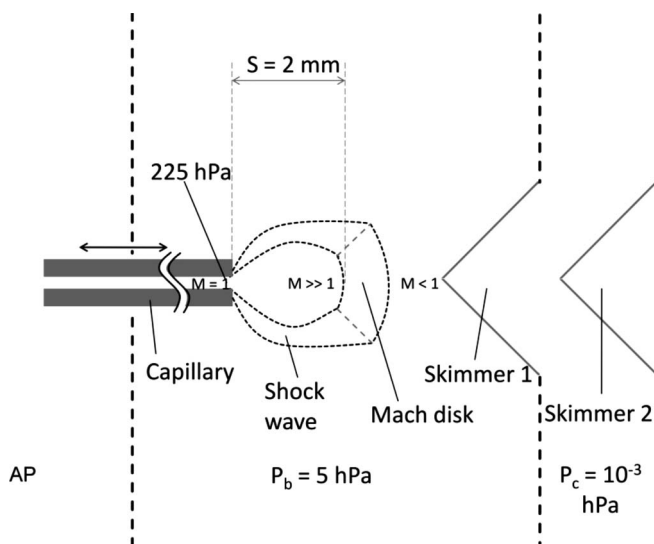


FIG. 3. A schematic drawing of the capillary outlet and the differential pumping stage. The expansion with the position of the Mach disk is sketched. Additionally, the pressures in the pumping stages are shown.

formation is limited by the collision number. The number of bimolecular collisions in the expansion is proportional to $P_0 \times d/T_0$, with T_0 as the temperature and P_0 as the pressure of the gas before the expansion, and d as the inner diameter of the nozzle. For the clustering processes intermolecular collisions are required and in the expansion these collisions are proportional to $P_0^2 \times d/T_0^2$. However, the molecules move essentially collision free after a few nozzle diameters, after which they remain in their energy state (i.e., “freeze in”).¹⁵ The terminal Mach number M_t is calculated with Eq. (2). K_n is the Knudsen number, defined as the mean free path of the gas before the expansion divided by the nozzle diameter.²⁰ Neither the comparison between the theoretical and the measured water cluster distribution nor the change of the nozzle design makes a significant influence on the cluster distribution. For details of the nozzle design and effects on the transmission efficiency see Sec. VI:

$$M_t = 1.17K_n^{((1-\gamma)/\gamma)}, \quad (2)$$

$$T_t = \frac{T_0}{1 + ((\gamma - 1)M_t^2)/2}. \quad (3)$$

The temperature T_t reached in an expansion at a certain Mach number is calculated with Eq. (3). It depends on the temperature T_0 of the gas before expansion, the Mach number M , and the heat capacity ratio γ . With the terminal Mach number, Eq. (3) can be used to calculate the minimal temperature reached in the expansion before entering the collision free region.

The so-called Mach disk is the shock area where the molecules collide with the background gas in the vacuum system (P_b in Fig. 3) and decelerate to a speed smaller than the speed of sound. The distance S to the nozzle is given by empirical equation (4):¹⁵

$$S = 0.67d \left(\frac{P_0}{P_1} \right)^{1/2}. \quad (4)$$

S depends on the pressure before the expansion P_0 and the pressure after the expansion P_1 . The Mach disk has a thickness of the order of the mean free path in the vacuum system. Within the Mach disk region fractions of the directed kinetic energy are converted back into the thermal motion of the gas, resulting in an increase in the static temperature of the gas. Further, typical parameters for the expansions in the present vacuum system are given in Table I.

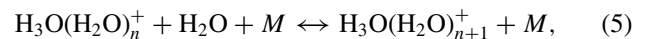
B. Comparison with a thermodynamic model

Fig. 4 shows the transition from the thermal sampling mode (5 hPa) to an expansion cooled cluster distribution (15 hPa). For these measurements the background pressure at the exit port of the capillary was changed (5, 10, and 15 hPa, respectively) but the mixing ratios were held constant. A distance of 6 mm between the capillary and the skimmer was chosen. The total flow was held constant, with a butterfly valve that adjusts the throughput of the rotary vane pump evacuating the first pumping stage. To evaluate the measured cluster distribution, a thermodynamic model was set up that

TABLE I. The calculated parameters of the first two expansions in the mass spectrometer.

	Outlet capillary	Outlet skimmer 1
Experimental parameters		
P_0 (hPa)	255	5
P_1 (hPa)	5	1×10^{-3}
λ_0 (mm)	3.1×10^{-4}	1.4×10^{-2}
d (mm)	0.5	0.8
γ		1.4
T_0 (K)		295
Calculated values		
S (mm)	2.4	39
K_n	6.2×10^{-3}	1.8×10^{-2}
M_t	8.3	3.0
T_t (K)	20	105

represents the conditions present after the Mach disk. The parameters used for the thermodynamic model were calculated from the equilibrium constants determined by Lau *et al.*⁶ and Kebarle *et al.*⁴ A comparison between the thermodynamic model and the measured water cluster distribution shows that the cluster distribution is in agreement at 5 hPa for a water mixing ratio of 0.3 vol.%. At 10 hPa changes in the cluster distribution are observed, which are caused by additional nucleation in the cold expansion. The spectrum at 15 hPa is plotted in Fig. 4 and exhibits a broad non-thermal cluster distribution caused by the nucleation process in the second expansion:



$$\Delta G = \Delta H - T \times \Delta S, \quad (6)$$

$$K_p = e^{\Delta G/R \times T}, \quad (7)$$

$$K_c = K_p \times R \times T/N_A, \quad (8)$$

$$\begin{aligned} & \log[\text{H}_3\text{O}(\text{H}_2\text{O})_n^+] \\ &= \sum_{i=1}^n \log K_i + (n-1) \log[\text{H}_2\text{O}] + \log[\text{H}_3\text{O}^+]. \end{aligned} \quad (9)$$

The equilibrium constants used for the thermodynamic model are shown in Table II. They are calculated using Eqs. (6)–(8), at a temperature of 295 K. Equation (9) is derived from the equilibrium equations and represents the cluster concentrations in thermal equilibrium when starting with a known H_3O^+ concentration.

In the negative ion mode $[\text{O}_2(\text{H}_2\text{O})_n]^-$ clusters are a product of the ionization by electrons expelled by toluene. The distribution of these clusters has also been compared with rate constants²¹ found in the literature, which confirms the thermal equilibrium distribution of the clusters.¹¹

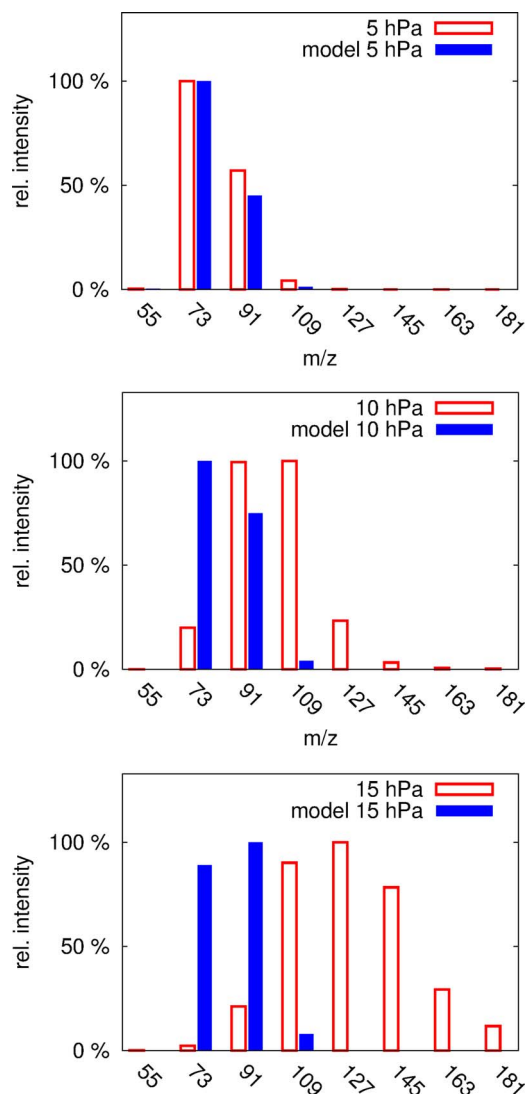


FIG. 4. Normalized intensity of the measured water cluster signals at different pressures in the first pumping stage. The solid bars give the water cluster distribution calculated in the thermodynamic model. The water mixing ratio is 0.3 vol.%. Each spectrum has been scaled such that the most intensive peak is equal to 100%.

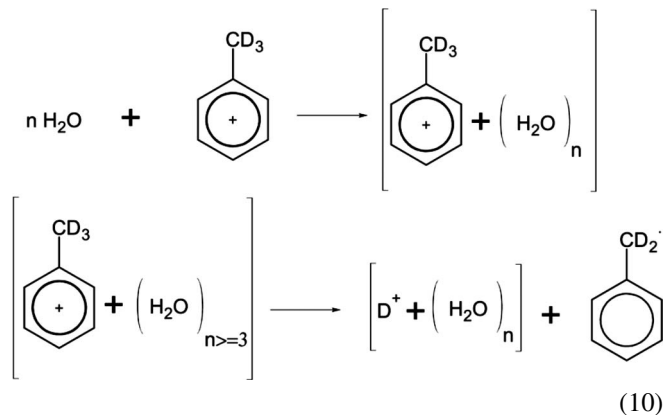
TABLE II. The equilibrium constants used for the thermodynamic model of the water clusters are estimated using ΔH and ΔS , which are measured by Lau *et al.*⁶ and Kebarle *et al.*⁴ The parameter n is referred to Eq. (5).

$n, n+1$	ΔH (kcal/mol)	ΔS (cal/(K mol))	K_c (295 K) (1/cm ³)
0, 1	31.6	24.3	5.08×10^{-2}
1, 2	19.5	21.7	2.04×10^{-10}
2, 3	17.9	28.4	4.56×10^{-13}
3, 4	12.7	23.4	7.93×10^{-16}
4, 5	11.6	25	5.43×10^{-17}
5, 6	10.7	26.1	6.72×10^{-18}
6, 7	11.7	29.6	6.36×10^{-18}
7, 8	10.3	27	2.16×10^{-18}

IV. DISCUSSION

A. Ionization

The proton transfer from the toluene radical cation to water molecules is described in the literature.²² In this study, additional measurements were made with deuterated toluene proving that the proton is transferred to ion clusters.



B. Gas temperature and cluster size distribution

In order to study the dependence of the cluster size distribution on the gas temperature mass spectra were taken with the capillary held at room temperature and at elevated temperature. These experiments were performed with a 0.3 vol.% water vapor mixing ratio at a pressure of 10 hPa. A thermocouple was placed on the outer wall of the capillary about 5 cm upstream of the exit, resulting in an overestimation of the effective gas temperature due to the colder tip of the capillary and the cooling effect of the expansion. Figure 5 shows the cluster size distributions measured for temperature readings of 295 K and 490 K. These are compared to the simulated cluster size distributions employed in the thermodynamic model (cf. 5). This comparison shows that the capillary at room temperature for the experimental distribution is best matched by a cluster size distribution modeled for a 250 K gas temperature, while for the heated case the distribution is best matched with a temperature of 372 K. This is in good agreement with the assumptions made. Further studies could make temperature measurements within the gas stream after the capillary. However, this measurement might result in a bigger error due to the low pressure after the capillary.

A comparison between the two measurements shows that the total ion count decreased by 40% when heating the capillary and keeping the total mass flow into the capillary constant. However, this causes the pressure in the ion source to increase from 828 Torr (250 K) to 975 Torr (372 K). This effect is most likely caused by the dependence of fluid viscosity on the temperature.

C. Expansion

With sufficient intermolecular collisions the ions react with neutral molecules to form ion-bound clusters. By laterally moving the capillary the distance between the capillary and the skimmer was varied (see Fig. 3). Thus the

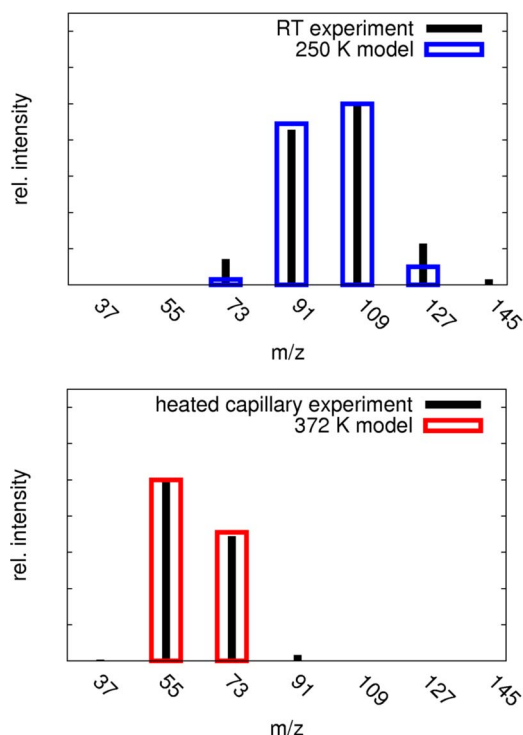


FIG. 5. Measured and estimated cluster distributions at temperatures indicated in each plot. The water mixing ratio is 0.3 vol.%.

probing position relative to the expansion and the Mach disk was changed. Downstream of the Mach disk the cluster distribution rapidly adjusts to the present thermal conditions. The clusters are smaller than those present in the ion source because of the pressure reduction from the ion source to the Mach disk.

To characterize the expansions after the capillary and skimmer 1, the parameters discussed in Sec. III A have been calculated (Table I). Experimentally observed cluster distributions generated by the expansion process that occurs after the capillary agree well with the predicted values. The position of the Mach disk calculated using Eq. (4) and the parameters in Table I (Outlet Capillary), is 2.4 mm downstream of the capillary exit, i.e., centered between the capillary and skimmer 1. Measurements have shown that there is a rapid decrease of the cluster size starting at a distance of 2.4 mm between the capillary and the skimmer, see Fig. 6. The measured position is in good agreement with the calculated position (2.4 mm) of the Mach disk. Additionally, Fig. 6 shows the mean cluster distribution at 6 hPa. The Mach disk position estimated is 2.2 mm at 6 hPa, which fits with the data. Fig. 6 also shows that the cluster distribution needs approximately 2 mm to adjust to the local conditions. The capillary was thus adjusted to a distance of 6 mm upstream of skimmer 1 for the thermal sampling mode, which kept skimmer 1 downstream of the Mach disk during this pumping stage when pressures are 5 hPa and higher.

Further, a change in the absolute signal intensity with an increase in the distance is clearly seen in Fig. 6. For this measurement radical toluene ions are generated by a krypton-vacuum ultraviolet lamp (Waters Corporation, Milford, USA, APPI lamp) because of the enhanced ion production stability

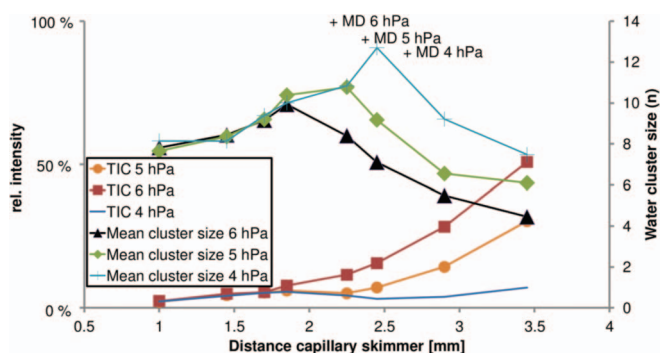


FIG. 6. The measured relative signal intensities and the signal weighted water cluster size average at different pressures in the first pumping stage for a particular distance between the capillary and skimmer 1. The water mixing ratio is 0.16 vol.%. “+” marks the estimated position of the Mach disk.

that is available while moving the capillary. At shorter distances each signal is lower because many cluster species arise during the cold expansion. Also the total ion count is two orders of magnitude lower compared to the sampling in the thermal sampling mode. At the position of the Mach disk, a sharp increase in the signal intensity is observed probably associated with a change in the fluid dynamics. After the Mach disk the signal increases further until the optimal position is reached. The water cluster distribution has reached its thermal equilibrium 6 mm downstream the capillary at pressures of 5 and 10 hPa as obvious from Fig. 4. Fig. 7 illustrates the fast change in the water cluster distribution after the Mach disk.

D. Thermal sampling

Many cluster processes have been studied using effusive nozzles.¹⁵ The disadvantage of this measurement technique is the small orifice required since it limits the ion flow into the mass analyzer. An alternative approach for measuring the cluster distribution is what we call the “thermal sampling mode.” Searcy and Fenn²³ reported that they found relatively small clusters using a non-effusive sampling nozzle, although clusters should grow in the cold expansion region. Later, Zook and Grimsrud²⁴ found that they can measure the thermal equilibrium cluster distribution without an effusive

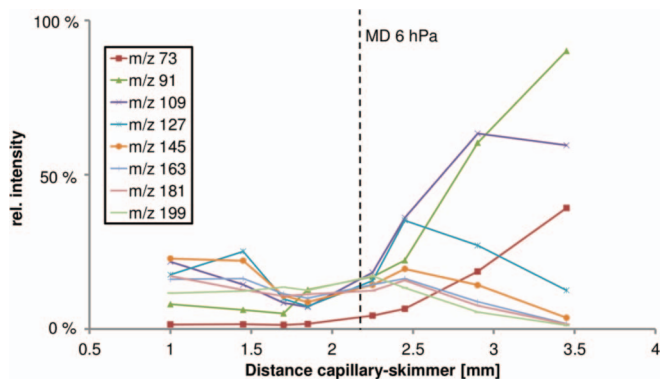


FIG. 7. The measured relative signal intensities at 6 hPa, during the first pumping stage, as a function of the distance between the capillary and skimmer 1. The water mixing ratio is 0.16 vol.%. The dashed line marks the estimated position of the Mach disk.

nozzle. But they were limited to specific parameters, e.g., an elevated temperature and He buffer gas.

In this study clusters produced in the ion source are sampled via a capillary. In the expansion after the capillary the water clusters nucleate with neutrals and lose these neutrals again in the Mach disk and in following collisions. If no nucleation process is initiated in the second expansion, then it is possible to sample the thermally re-equilibrated cluster distribution produced after the first Mach disk. For this re-equilibrated cluster distribution we assume the same gas temperature as in the capillary, as supported by our measurements (cf. Sec. III B and the poster of Klopotoski *et al.*²⁵).

Initially water clusters are produced by association reactions in the ion source. These reactions are fast and are completed in at least 100 μs .²⁶ Additionally, further cluster growth and production can occur via nucleation in the expansion (cf. Hagena²⁷ and Castleman and Keesee²⁸). Hagena²⁷ calls these bigger clusters metastables, indicating that the nucleation process is rapidly inverted. Nucleation occurs in the expanding gas at the capillary outlet because a low temperature is reached in this expansion. The measured size distribution decrease is attributed to the presence of the Mach disk in the first expansion. The distance between the capillary and the skimmer needs to be increased for cluster reactions slower than the water cluster formation causing a re-equilibration of the clusters. The current assembly is limited to a maximum distance of 6 cm between the capillary and skimmer 1. The capillary jet generates a directed gas stream in the direction of the skimmer,²⁵ so even at larger distances no significant signal loss is expected.

In the thermal sampling mode nucleation processes in the second expansion are avoided. Nucleation becomes possible whenever the partial pressure of a compound exceeds the vapor pressure of the condensed phase for the given temperature.²⁸

Measurements have been made with a water vapor mixing ratio of 1300 ppmV (at 5 hPa in the first pumping stage), a number derived from the mixing ratio of the ion source. These measurements show that this value is right below the threshold of nucleation, however, doubling the pressure results in nucleation (cf. Fig. 9). Both measurements have been made at low terminal temperatures in the second expansion estimated by an empirical equation (cf. Sec. III A). The critical water concentration for the nucleation is estimated using the empirical vapor pressure equation for the water vapor pressure above ice, as measured by Marti and Mauersberger.²⁹ Comparing the critical water concentration with a given water concentration shows that nucleation should occur in both measurements in the second expansion. We conclude that under certain conditions (cf. Fig. 9) the time for the second expansion is too short for nucleation since the collision frequency in the second expansion rapidly drops to zero. The mean free path after the second expansion (10⁻³ hPa) is higher than the distance between the nozzles. Higher pressure in front of skimmer 1 (10 hPa) in the second measurement reduces the nucleation time and results in bigger water clusters. This behavior has been modeled,³⁰ however, a detailed study should be subject of a forthcoming publication.

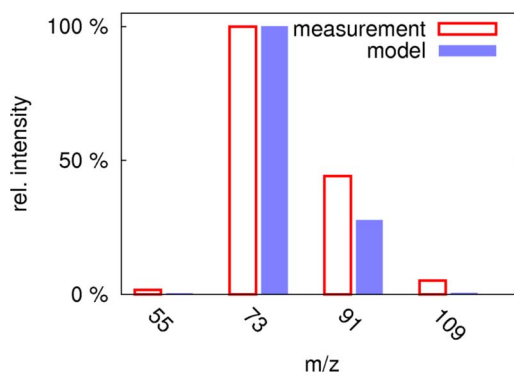


FIG. 8. Relative intensities of the measured water cluster signals at 15 hPa after the capillary compared with water cluster distribution for this pressure calculated by the thermodynamic model. The water mixing ratio is 300 ppmV.

At higher pressures the nucleation time in the second expansion should be increased and should employ smaller water mixing ratios in order not to change the thermal cluster distributions. Figure 8 shows such a measurement at 15 hPa in the first pumping stage and a water vapor mixing ratio of 300 ppmV, which results in a thermally equilibrated cluster distribution. An overview of the nucleation-free measurements is given in Figure 9. Details of nucleation processes that occur during the expansion are given by Gordon *et al.*³¹ Here just a rough estimate is made to demonstrate that the theory fits with the measurements. The temperature and pressure drop during the expansion resulting in a slower water cluster production. The forward reaction rate for the water cluster production is 10⁻²⁹ molecules⁻² cm⁶ s⁻¹ at 300 K.³² Because water is in excess compared to the cluster ions it is possible to estimate the pseudo first order relaxation time for the water clusters. Using a water mixing ratio of 1300 ppm the relaxation time is 4 × 10⁻⁴ s for 15 hPa and 3 × 10⁻³ s for 5 hPa. The time the gas spends between the two skimmers is approximately 1 × 10⁻⁴ s. This clearly demonstrates a change from a thermal cluster distribution to nucleation when increasing the pressure from 5 hPa to 15 hPa.

The nucleation for water vapor in the expansions is characterized, showing the borders of the thermal sampling mode for water. Different vapors present in the expansion will call for further analysis due to their different nucleation rates.³³

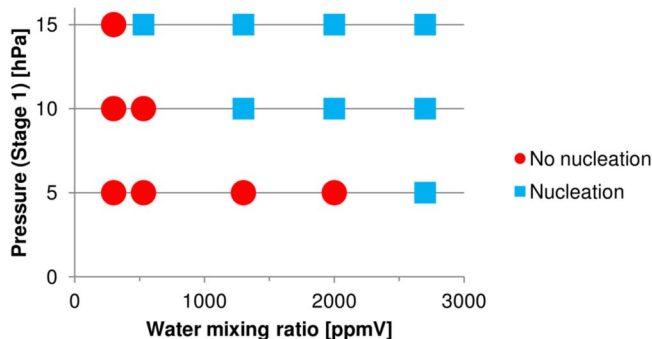


FIG. 9. Background pressure in the first pumping stage plotted against the water mixing ratio in the ion source. The quadrat indicates measurements with nucleation during the second expansion, which changes the measured cluster distribution.

V. COLLISION-INDUCED DISSOCIATION

A. Theory

In most API mass spectrometers, additional energy is transferred to the ions by electrostatic fields. These electrostatic fields accelerate the ions to kinetic energies exceeding their dissociation threshold and inducing dissociation upon the next collision. Further, the elevated collision energy from the electrostatic fields may drive additional reactions, e.g., the production of protonated species.³⁴ Collisions driven by electrostatic fields deliver energy to the chemical system causing an elevated effective ion temperature. Moreover, the ion velocity distribution becomes non-Maxwellian due to the directional character of electrostatic fields, hence only an effective temperature can be estimated.²⁸ For cluster ions the dissociation threshold is comparatively low. The “critical” pressure region is located between low pressures where not enough collision partners are present (10^{-5} hPa⁸) and pressures, where the mean free path becomes too short for sufficient acceleration. This region is exploited for analytical purposes in the MS/MS experiments as well for its efficient declustering. However, moderate fields are also a viable tool for studying the composition of ion-bound clusters. For simplification the above mentioned processes are summarized as collision-induced dissociation.

B. Results

The transfer stage of the present setup has been optimized to minimize CID processes when in “thermal sampling mode”. This was shown experimentally (cf., e.g., Fig. 4). In addition, controlled CID experiments for the different pressure regimes were performed. By applying voltages to the electrodes in the respective pumping stages changes in the cluster size distribution were monitored. All CID experiments shown here were performed with a water mixing ratio of 0.12 vol.%. The pumping stage downstream of the capillary was held at a pressure of 10 hPa, resulting in a background pressure of 10^{-3} hPa in the following pumping stage. CID at 10 hPa was driven with a potential at the capillary tip and with grounded skimmers. The applied field gradient between the capillary and skimmer 1 was varied from 0 to 950 V/cm. Due to the short mean free path relatively high voltage gradients are required to induce the CID processes. At field gradients of 330–475 V/cm the maximum of the water cluster distribution was reduced from $n = 4$ to $n = 3$. A field gradient of 1000 V/cm resulted in a water cluster distribution with the size of $n = 0 \dots 2$, with a maximum intensity at $n = 2$.

CID at 10^{-3} hPa was driven with a grounded skimmer 2 and the same elevated potential at the capillary tip and skimmer 1. The gas density is much lower, thus much lower voltages are required to drive the CID processes in this pressure region. Without electrostatic fields the ions spend less than 100 μ s between the skimmers with a mean free path higher than the distance between the nozzles. At this pressure, favorable CID field gradients are in the range of 0 to 10 V/cm. The reduction of the cluster size with the potential between the skimmers is shown in Fig. 10. Below 1.25 V/cm no apprecia-

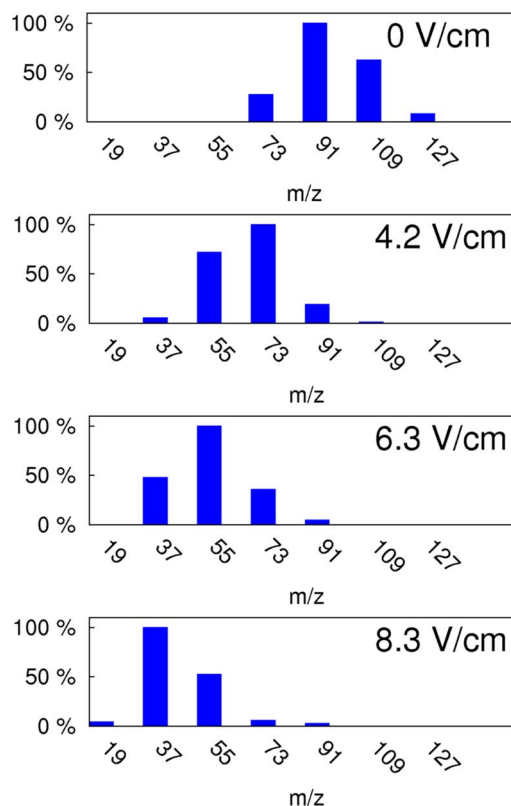


FIG. 10. Relative intensity of the measured water clusters as a function of the different CID voltages between the two skimmers.

ble CID effects have been recorded. At field gradients exceeding 8 V/cm the first $[M - H]^+$ toluene fragments as well as the production of N_2^+ ions have been observed. At field gradients of 17 V/cm these peaks show intensities that are equal to those of the toluene $[M]^+$ peak. It is reasonable to assume that higher field gradients are reached at the sharp skimmer tip, as judged from the observed nitrogen ion signals.

Without electrostatic fields present it is possible to record radical cation multimers as well as ion bound clusters. These multimers and clusters are obviously present in the ion source. An example is the toluene radical cation dimer which is easily decomposed using electrical fields of the order of 16 V/cm (cf. Fig. 11). For measurements of the toluene spectra the distance between the capillary and skimmer 1 has been increased to the maximum allowed by the construction (6 cm) such that it gives the toluene time to equilibrate. Measurements with a distance of 1 cm between the capillary and skimmer 1 under similar conditions shows no significant difference. Moving the capillary gives an idea of the magnitude of the reaction rates involved. The convergence with increasing distance between capillary and skimmer shows that an equilibrium is reached. However, rate constants and nucleation rates of the toluene multimers that are produced during the second expansion are not found in the literature and thus it cannot be checked for nucleation. Ernstberger *et al.*³⁵ measured a dissociation energy of 660 meV for the toluene radical cation dimer indicating that the dimer is stable under the conditions in the ion source. Because no bigger toluene clusters were measured we are certain that we are very close to the thermal

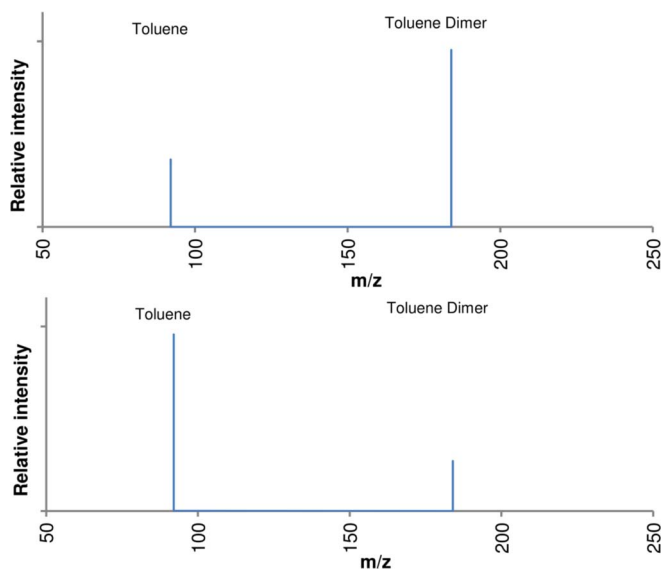


FIG. 11. Mass spectrum of toluene at thermal sampling conditions (top) and 16 V/cm (bottom). The pressure after the capillary is 15 hPa and the mixing ratio of toluene is 480 ppm.

equilibrium toluene cluster distribution as long as no other nucleation processes are involved.

VI. INSTRUMENT OPTIMIZATION

In this section, we briefly illustrate the changes implemented for the second generation instrument. These changes mainly address an improved ion transfer within the pumping stage between the skimmers. The measurements discussed so far were performed with the first generation instrument.

The two skimmer assembly has been replaced by a skimmer orifice plate assembly (Fig. 12). The orifice of skimmer 1 has been reduced to 0.6 mm to reduce the terminal temperature in the expansion, thus increasing the pressure and concentration range for the thermal sampling mode. Skimmer 2 was substituted by an orifice plate (ID 2 mm). The orifice plate is isolated using a ceramic mount and may be biased. An additional plate electrode mounted between the first skimmer and the orifice plate creates a lens assembly. The plate electrode is made of stainless steel with a 1 cm inner diame-

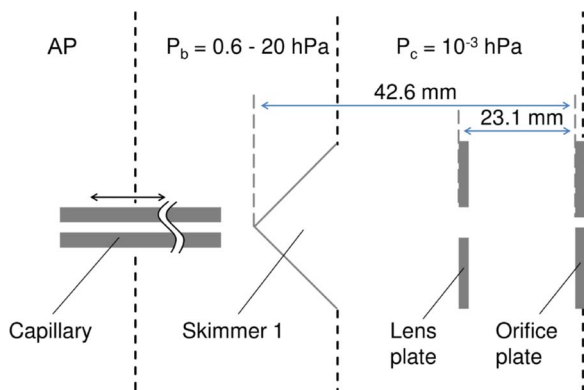


FIG. 12. A schematic drawing of the skimmer orifice plate assembly.

ter. The distance between the orifice plate and the lens plate is 23.1 mm.

Using skimmers results in a sharp electrostatic field gradient as discussed in Sec. V B. Such field gradients cause, for example, the ionization of N_2 with only a 15 V potential difference between the two skimmers of the 1st generation assembly. Measurements with the new assembly caused no ionization of N_2 with a potential difference of up to 30 V over a similar distance.

Compared to the second generation set-up, with no electrostatic fields present, the two skimmer assembly in the first generation shows that the transmission is a factor 2–4 times better. However, less than a factor of 5 can be gained in the first generation when electrostatic fields are applied to the skimmers during the thermal sampling mode but before considerable CID processes are invoked. The skimmer orifice nozzle assembly demonstrates a greatly improved ability to focus ions. Without changes in the cluster distribution, i.e., in “thermal sampling mode,” a factor of approximately 20 is gained by applying a small potential between the skimmer and the nozzle. This factor increases to approximately 50 (as compared to grounded electrodes) when voltages are increased further, however, at the expense of CID, as indicated by the change in the cluster distribution. These results show that combining electrostatic and fluid dynamic simulations in this region will help to further improve the ion transmission efficiency. Poor signal intensities of skimmer assemblies have also been observed earlier, see, e.g., Bruins *et al.*⁸

To ensure that no CID occurs in the region downstream of the orifice plate we compared measurements under otherwise identical conditions but using different orifice diameters. These measurements showed no changes in the cluster distribution with orifice diameters of 2, 1, and 0.5 mm.

VII. CONCLUSION

The transfer stage of the mass spectrometer has been developed, optimized, and characterized for the measurement of the cluster distributions that closely resemble those in the API source.

The inlet is designed to have the ability to vary important experimental parameters, e.g., the various electrostatic fields present. For example, the distance and the pressure between the first nozzle and the inlet capillary can be adjusted for optimal sampling. The distance between the first nozzle and the inlet capillary needs to be large enough to re-equilibrate the cluster distribution after the Mach disk of the first expansion. The partial vapor pressure of the neutral cluster ligands, e.g., water, should be a low enough value such that the cluster species can be mass spectrometrically detected without noticeable nucleation. Critical parameters for the measured cluster distribution have been identified and compared with a thermodynamic model, demonstrating that the cluster distribution is thermally equilibrated.

The transfer stage offers the opportunity to study the processes during the expansion. Additionally, it can implement or not implement CID for the analysis of the cluster composition in the thermal sampling mode.

The inlet capillary can be combined with most AP ion sources. The mass spectrometer has no mass discriminating RF optics and thus can measure low mass to charge ratios.

ACKNOWLEDGMENTS

We would like to acknowledge the work of Ronald Giese, University of Wuppertal and Jochen Barthel, Forschungszentrum Jülich GmbH who helped to realize and construct the scientific instrument used in this study. We thank TOFWERK AG for their great support. S.A. thanks the workgroup at the University of Wuppertal for granting use of the mass spectrometer laboratory for one year.

- ¹D. B. Robb, T. R. Covey, and A. P. Bruins, *Anal. Chem.* **72**, 3653 (2000).
- ²S. Schmidt, M. F. Appel, R. M. Garnica, R. N. Schindler, and T. Benter, *Anal. Chem.* **71**, 3721 (1999).
- ³D. Robb and M. Blades, *J. Am. Soc. Mass Spectrom.* **16**, 1275 (2005).
- ⁴P. Kebarle, S. K. Searles, A. Zolla, J. Scarboro, and M. Arshadi, *J. Am. Chem. Soc.* **89**, 6393 (1967).
- ⁵M. W. Siegel and W. L. Fite, *J. Phys. Chem.* **80**, 2871 (1976).
- ⁶Y. K. Lau, S. Ikuta, and P. Kebarle, *J. Am. Chem. Soc.* **104**, 1462 (1982).
- ⁷H. Kersten, V. Derpmann, I. Barnes, K. Brockmann, R. O'Brien, and T. Benter, *J. Am. Soc. Mass Spectrom.* **22**, 2070 (2011).
- ⁸A. P. Bruins, *Mass Spectrom. Rev.* **10**, 53 (1991).
- ⁹V. V. Pervukhin, *J. Anal. Chem.* **63**, 1182 (2008).
- ¹⁰V. J. Caldecourt, D. Zakett, and J. C. Tou, *Int. J. Mass Spectrom. Ion Process.* **49**, 233 (1983).
- ¹¹V. Derpmann, S. Albrecht, and T. Benter, *Rapid Commun. Mass Spectrom.* **26**, 1923 (2012).
- ¹²S. Klee, S. Albrecht, V. Derpmann, H. Kersten, and T. Benter, *Anal. Bioanal. Chem.* **405**, 6933 (2013).
- ¹³H. Kersten, Ph.D. thesis, University of Wuppertal, 2011, <http://nbn-resolving.de/urn/resolver.pl?urn=urn:nbn:de:hbz:468-20110418-092806-6>.
- ¹⁴I. Barnes, H. Kersten, W. Wissdorf, T. Pohler, H. Honen, S. Klee, K. Brockmann, and T. Benter, "Novel laminar flow ion source for LC- and GC-API MS," in 58th ASMS Conference on Mass Spectrometry and Allied Topics, Salt Lake City, UT, USA, 2010.
- ¹⁵*Atomic and Molecular Beam Methods*, edited by G. Scoles (Oxford University Press, New York, USA, 1988), Vol. 1.
- ¹⁶A. Michalke, *Ingen. Arch.* **57**, 377 (1987).
- ¹⁷M. Wutz, H. Adam, and W. Walcher, *Theorie und Praxis der Vakuumtechnik* (Friedr. Vieweg und Sohn, 1988), Vol. 4.
- ¹⁸*Simion* (Scientific Instrument Services Inc., 8.0), www.simion.com.
- ¹⁹S. Wuetrich, TOFWERK AG, Uttigenstrasse 22, 3600 Thun, Switzerland, private communication (2011), www.tofwerk.com.
- ²⁰J. B. Fenn, *Int. J. Mass. Spectrom.* **200**, 459 (2000).
- ²¹J. D. Payzant and P. Kebarle, *J. Chem. Phys.* **56**, 3482 (1972).
- ²²S. Li and E. R. Bernstein, *J. Chem. Phys.* **97**, 792 (1992).
- ²³J. Q. Searcy and J. B. Fenn, *J. Chem. Phys.* **61**, 5282 (1974).
- ²⁴D. R. Zook and E. P. Grimsrud, *J. Phys. Chem.* **92**, 6374 (1988).
- ²⁵S. Klopotoski, Y. Brachthaeuser, D. Mueller, H. Kersten, W. Wissdorf, V. Derpmann, K. J. Brockmann, U. Janoske, and T. Benter, "API-MS transfer capillary flow: Examination of the downstream gas expansion," conference poster presented at 59th ASMS Annual Meeting, Denver, 2011.
- ²⁶P. Kebarle *Ion-Molecule Reactions*, edited by J. L. Franklin (Plenum, New York, USA, 1972), Chap. 7.
- ²⁷O. F. Hagen, *Rev. Sci. Instrum.* **63**, 2374 (1992).
- ²⁸A. W. Castleman and R. G. Keesee, *Chem. Rev.* **86**, 589 (1986).
- ²⁹J. Marti and K. Mauersberger, *Geophys. Res. Lett.* **20**, 363, doi:10.1029/93GL00105 (1993).
- ³⁰A. A. Vostrikov and D. Y. Dubov, *J. Exp. Theor. Phys.* **98**, 197 (2004).
- ³¹R. J. Gordon, Y. T. Lee, and D. R. Herschbach, *J. Chem. Phys.* **54**, 2393 (1971).
- ³²A. N. Hayhurst and N. R. Telford, *Proc. R. Soc. London, Ser. A* **322**, 483 (1971).
- ³³A. A. Lushnikov and A. G. Sutugin, *Russ. Chem. Rev.* **45**, 197 (1976).
- ³⁴J. A. Syage, *J. Am. Soc. Mass Spectrom.* **15**, 1521 (2004).
- ³⁵B. Ernstberger, H. Krause, and H. J. Neusser, *Z. Phys. D* **20**, 189 (1991).